Impact of the gut microbiome on nicotine's motivational effects and glial cells in the ventral tegmental area in male mice

Alina Lakosa, Anaïs Rahimian, Flavio Tomasi, Fabio Marti, Lauren Reynolds, Léa Tochon, Vincent David, Anne Danckaert, Candice Canonne, Sylvana Tahraoui, et al.

Impact of the gut microbiome on nicotine's motivational effects and glial cells in the ventral tegmental area in male mice

Alina Lakosa[1,9] MSc, Anaïs Rahimian[1,9] MSc, Flavio Tomasi[1,7,9] MSc, Fabio Marti[2] PhD, Lauren Reynolds[2] PhD, Léa Tochon[3,4] PhD, Vincent David[3,4] PhD, Anne Danckaert[5] PhD, Candice Canonne[1] MSc, Sylvana Tahraoui[1] BSc, Fabrice De Chaumont[6] PhD, Benoît Forget[1,8] PhD, Uwe Maskos[1] DPhil, Morgane Besson[1]* PhD

[1]Institut Pasteur, Université de Paris, Neurobiologie Intégrative des Systèmes Cholinergiques, CNRS UMR 3571, Paris, France
[2]Plasticité du Cerveau, CNRS UMR 8249, ESPCI Paris, Université PSL, Paris, France
[3]Université de Bordeaux
[4]CNRS UMR 5287, Institut de Neurosciences Cognitives et Intégratives d'Aquitaine, Bordeaux, France
[5]UTechS Photonics Bioimaging/C2RT, Institut Pasteur, 25 rue du Dr Roux, 75724 Paris Cedex 15, France
[6]Génétique humaine et fonctions cognitives, CNRS UMR 3571, Institut Pasteur, 25 rue du Dr Roux, 75724 Paris Cedex 15, France
[7]Present address: Neuroscience Paris Seine, Institut de Biologie Paris Seine, Sorbonne Université, INSERM, CNRS, Paris, France
[8]Present address: Génétique humaine et fonctions cognitives, CNRS UMR 3571, Institut Pasteur, 25 rue du Dr Roux, 75724 Paris Cedex 15, France
[9]These authors contributed equally

Corresponding author:

Morgane Besson
Neurobiologie Intégrative des Systèmes Cholinergiques
Institut Pasteur
25 rue Dr Roux
75015 Paris
France
+33140613777
morgane.besson@pasteur.fr

Abstract

A link between gut dysbiosis and the pathogenesis of brain disorders has been identified. A role for gut bacteria in drug reward and addiction has been suggested but very few studies have investigated their impact on brain and behavioral responses to addictive drugs so far. In particular, their influence on nicotine's addiction-like processes remains unknown. In addition, evidence shows that glial cells shape the neuronal activity of the mesolimbic system but their regulation, within this system, by the gut microbiome is not established. We demonstrate that a lack of gut microbiota in male mice potentiates the nicotine-induced activation of sub-regions of the mesolimbic system. We further show that gut microbiota depletion enhances the response to nicotine of dopaminergic neurons of the posterior ventral tegmental area (pVTA), and alters nicotine's rewarding and aversive effects in an intra-VTA self-administration procedure. These effects were not associated with gross behavioral alterations and the nicotine withdrawal syndrome was not impacted. We further show that depletion of the gut microbiome modulates the glial cells of the mesolimbic system. Notably, it increases the number of astrocytes selectively in the pVTA, and the expression of postsynaptic density protein 95 in both VTA sub-regions, without altering the density of the astrocytic glutamatergic transporter GLT1. Finally, we identify several sub-populations of microglia in the VTA that differ between its anterior and posterior sub-parts, and show that they are re-organized in conditions of gut microbiota depletion. The present study paves the way for refining our understanding of the pathophysiology of nicotine addiction.

Introduction

The gut hosts trillions of microbes that are key players in host physiological processes [1]. Over the past decade, it has become clear that the microorganisms inhabiting the gastrointestinal tract have a critical role in orchestrating brain functions and behavior [2]. A complex bidirectional network exists between the gut microbiome and the brain, involving various bacterial structural components and metabolic products as signaling agents [2,3]. Many different environmental factors influence the composition of the gut microbiome and can cause dysbiosis, a microbial imbalance that can be rescued notably by probiotics [2]. Numerous studies have identified a link between gut dysbiosis and the pathogenesis of several neuropsychiatric disorders [2].

While emerging evidence suggests a role for gut bacteria in the pathophysiology of drug addiction [4], studies of their impact on brain and behavioral responses to addictive drugs have been very limited so far. Tobacco smoking is responsible for more than seven million deaths each year [5]. Considering the low success rates of the currently available therapies for tobacco smoking cessation, there remains a significant need for novel therapeutic approaches [6]. Nicotine is the primary psychoactive substance of tobacco smoke responsible for its reinforcing and addictive properties [7]. Characterizing the potential influence of the gut microbiota on nicotine-induced reinforcement and brain alterations may provide a better understanding of the pathophysiology of nicotine addiction, in turn allowing the development of alternative intervention strategies.

The primary rewarding action of nicotine is mediated by the activation of the mesolimbic circuit, mainly composed of dopaminergic (DA) neurons that project from the ventral tegmental area (VTA) preferentially to the nucleus accumbens (NAcb) shell (NAcbS) [8-10]. It was recently demonstrated that gut microbiota alterations cause impaired plasticity in the VTA [11,12] and modulate cocaine reward [13,14] in mice, while gut hormones modulate drug rewarding properties [15]. However, the interplay between the gut microbiota and the mesolimbic system remains poorly defined. Although the mechanisms by which the gut microbiome impacts brain and behavior are not fully understood

so far, they have been shown to involve endocrine, neural and immune pathways. In particular, gut bacteria can impact the nervous system through microglia and astrocytes [16]. Importantly, glial activity has a crucial role in shaping the output of DA neurons and neuroimmune alterations were suggested as a key mechanism in substance use disorders [17]. A growing body of evidence suggests an influence of the microbiome on brain glia [18,19], yet, although impairments in microglia were recently characterized in several brain areas in mice in response to gut microbiota depletion [20,21], information concerning the consequences of gut microbiota alterations on the glial cells of the mesolimbic system is still lacking.

In this context, the main objectives of the present study were to examine the impact of gut microbiota on i) nicotine effects and ii) glial cells within the mesolimbic system.

Materials and Methods

All details are given in Supplementary Methods.

Animals

Mice were specific pathogen free (SPF) or germ free (GF) C57BL/6J males. All experimental procedures were performed in strict accordance with the Guide for the Care and Use of Laboratory Animals (NIH) and the European Commission regulations for animal use in research (CEE n° 86/609), and approved by the institutional Animal Care Committees of the French Ministry and of the Institut Pasteur.

Antibiotic (AB) treatments

For microbiota depletion, a cocktail of large-spectrum ABs (Sigma-Aldrich) composed of colistine (1 mg/ml; 27655), ampicilline (1 mg/ml; A9393), and streptomycine (5 mg/ml, S6501) in drinking water was used [21]. For parenteral AB administrations, mice were injected intraperitoneally (IP)

every day with 1% of the daily dose of the same cocktail dissolved in NaCl 0.9% (as previously described [13,22]).

Microbial DNA extraction and 16S rRNA sequencing

Fecal DNA was extracted using the ZR Fecal DNA MiniPrep kit (Zymo Research). Microbial profiling was assessed by 16S rRNA metagenomic analysis.

Behavioral assessment

Locomotor activity, anxiety-like behaviors and memory were assessed in SPF mice after ten days of AB oral exposure.

Measurement of nicotine-induced changes in brain c-Fos expression

SPF mice exposed to ABs for ten days through oral or parenteral administration, or GF mice ten days after their arrival in sterile isocages, and their controls, received an IP injection of (−)-nicotine bitartrate (Sigma-Aldrich) in 0.9% NaCl (0.5 mg/kg (free base)) or of 0.9% NaCl alone, after habituation to IP injections. Brains were extracted and processed for c-Fos immunofluorescence and quantification.

In vivo single cell juxtacellular recording of VTA DA neurons in response to nicotine

SPF mice exposed to AB oral exposure for ten days and their controls received intravenous (IV) administration of (−)-nicotine bitartrate (5, 7.5, 15, 30 or 60 µg/kg (salt)) or of 0.9 % NaCl. Spontaneous and nicotine-induced electrophysiological activity of VTA DA neurons was recorded.

Intra-VTA nicotine self-administration (SA)

Nicotine reinforcement was assessed as intra-VTA SA using a Y-maze discrimination task [23-25] with ten trials per session and one session per day in mice exposed to AB oral exposure for eight days beforehand and their controls. For each trial, each mouse had to choose between the nicotine-reinforced arm and the non-reinforced arm such that it could obtain a maximum of ten injections

per daily session. The interruption of photocell beams by the mouse entering the reinforced arm triggered a 50 nL intra-VTA injection of (−)-nicotine bitartrate. Because the photo beams were located only 6 cm from the end of each arm, the mouse had to enter an arm completely to end a trial.

For the first experiment, the increasing nicotine doses were 2, 10 and 50ng (salt) in 50nL of artificial cerebrospinal fluid (aCSF) per injection.

For the second experiment, the increasing nicotine doses were 50 and 500ng (salt) per injection. After the 10th session, the experiment was paused during 26 days during which, and until sacrifice, AB exposure was ceased for the mice previously AB-treated. Conversely, mice previously non AB-treated got exposed to ABs for eight days, before testing again both groups at the dose of 500ng. AB exposure was maintained in the newly AB-treated group until sacrifice.

Other groups of mice were trained at the dose of 0ng/50nL to control for possible effects of AB exposure on exploratory behaviors in the Y-maze.

The placements of the injection cannulas were confirmed by microscopic examination. Caeca were dissected out for size verification.

Nicotine withdrawal measurement

(−)-Nicotine bitartrate (10 mg/kg per day, free base) or NaCl 0.9% only solutions were administered through osmotic minipumps (model 2004, Alzet, Durect) for 28 days [26,27]. Oral exposure to ABs started as the same time as nicotine exposure and lasted for the whole time. To precipitate the withdrawal, mecamylamine hydrochloride (Sigma-Aldrich) was IP administered (2 mg/kg) [27].

Measurement of tyrosine hydroxylase (TH), glial fibrillary acidic protein (GFAP), post-synaptic density protein 95 (PSD-95) and glutamate transporter 1 (GLT1) expression

After ten days of AB oral treatment brains were extracted and processed for TH, GFAP, PSD-95 and GLT1 immunofluorescence and quantification.

Characterization of microglial populations

After ten days of AB oral treatment brains were extracted and processed for TH and Iba1 immunofluorescence. We performed a microglial morphology analysis based on phenotypic clustering as we previously described [28].

Experimental design and statistical analysis

The details of the n and statistical tests performed for each experiment are specified in the respective figure legend. Statistical analyses and results are recapitulated in Supplementary Tables 1-4 and 7. Statistical significance was set at $p<0.05$. All datasets generated and analysed are available in the G-Node repository. Hyperlink to datasets: Doi: 10.12751/g-node.f2vqud.

Results

AB-induced or constitutive gut microbiota depletion enhances nicotine-induced activation of the mesolimbic system

Submitting SPF mice to ABs [21] in drinking water for ten days resulted in a nearly complete depletion of the gut microbiota (**Table S1** for statistics), as indicated by enlarged caeca (**Fig1A**) [29], dramatically decreased fecal DNA concentration (**Fig1B**), 16S rRNA gene sequencing further showing that the composition of the very few microbiota remaining was altered (**Fig1C**) and PCoA of Bray-Curtis distances for bacterial communities showing a clustering of the different groups (**Fig1D**). We verified that such AB treatment would not have a major impact on a broad set of behaviors in separate groups of mice. AB mice displayed mildly decreased motor activity and memory while anxiety-like behaviors were not altered (**Fig.S1A-L, Table S1**).

We next assessed the expression of the immediate-early gene *c-fos* (**Table S1**), a marker of cell activation [30,31], in distinct areas of the mesolimbic system and other connected areas receiving DA input [32], following a single injection of nicotine (0.5 mg/kg, [31]) or of NaCl after ten days of AB (or water only) exposure (**Fig.1E-I**). We observed a group effect only for the i) posterior VTA (pVTA) [$H(3) = 16.47$, $p = 0.0009$] (**Fig.1E**), which is preferentially activated by nicotine compared

to the anterior VTA (aVTA) [31], ii) NAcbS [H(3) = 7.88, p = 0.048] (**Fig.1E**) and iii) interpeduncular nucleus (IPN) [H(3) = 7.85, p = 0.049] (**Fig.1F**) also implicated in nicotine addiction [33-36]. Remarkably, multiple comparisons showed that pVTA nicotine-induced activation was significant only in AB mice, while the NAcbS main group effect seemed supported by the AB-Nic group.

We next verified that these effects were actually due to AB local actions within the gut and not to unintended parenteral effects. In a new series of experiments mice were IP injected with the same AB cocktail (IP AB) (or with NaCl, IP Control) [13,22] every day for ten days before receiving an injection of nicotine or NaCl (**Table S1**). We quantified c-Fos levels in the mesolimbic system and IPN (**Fig.1J-K**). We observed a main group effect for the IPN [H(3) = 8.98, p = 0.029] without significant differences in pairwise multiple comparisons (**Fig.1K**). There was no enhanced nicotine-induced activation of the mesolimbic system in IP AB mice contrary to what we had seen in mice with oral AB exposure (**Fig.1J**). Parenteral exposure to AB did not alter caecum size (**Fig.1L**) or fecal DNA concentration (**Fig.1M**), or microbiota composition (**Fig.1C-D**).

Finally, we verified whether we would observe similar effects in a different model of gut microbiota depletion. We quantified c-Fos levels, in response to nicotine, in the mesolimbic system and IPN (**Fig.1N-O**) of GF mice as compared to SPF mice kept in comparable isolator cages for ten days (**Table S1**). We found a group effect for the pVTA [H(3) = 16.94, p = 0.0007], NAcbS [H(3) = 16.04, p = 0.001], NAcb core (NAcbC) [H(3) = 9.71, p = 0.021] (**Fig.1N**) and IPN [H(3) =24.76, p < 0.0001] (**Fig.1O**). Multiple comparisons showed that nicotine-induced activation of the pVTA and NAcbS was significant only in GF mice, while the NAcbC main group effect was supported by the GF+Nic group. Nicotine-induced activation of the IPN was significant in both SPF and GF mice.

These data support the idea that the absence of gut microbiota enhances the stimulation of the core regions of the mesolimbic system induced by nicotine.

Gut microbiota depletion enhances nicotine activation of DA neurons in the pVTA.

We next recorded *in vivo* the electrophysiological properties of identified VTA DA neurons, under baseline conditions and in response to IV injections of nicotine [8,9], in mice after ten days of AB (or water) exposure (**Table S2** for statistics). We took advantage of juxtacellular labeling to analyze

separately neurons of aVTA and pVTA **(Fig.2A)**. We did not observe any differences between groups in pVTA DA neurons' spontaneous activity (**Fig.2B**). DA neurons increased their activity in response to nicotine in a dose-dependent manner [$F(dose)_{6,168} = 13$, $p < 0.0001$] (**Fig.2C-E**). We determined a population-level response threshold by comparing the change in firing induced by saline with that induced by each dose of nicotine. pVTA DA neurons of control mice significantly increased their firing frequency from the dose of 15 µg/kg, while there was a left-shift in the dose response curve in AB mice whose neurons started responding at lower doses, including 5, 7.5 and 10 µg/kg [doses 5 to 10 µg/kg: $F(group)_{1,72} = 4.587$, $p = 0.036$] (**Fig.2D-E**). These results suggest that AB treatment increases the excitability of pVTA DA neurons in response to nicotine at the individual level. We therefore compared the proportion of significantly nicotine-activated neurons between groups for each dose. The ratio of active cells in AB mice was significantly increased for the lowest doses of nicotine (5 to 10 µg/kg), but not for the highest ones. AB treatment did not significantly alter the response of DA neurons to nicotine in the aVTA (**Fig.S2A-B**).

Gut microbiota depletion alters nicotine's motivational effects in the intra-VTA SA procedure

We next aimed to test the hypothesis that gut microbiota depletion would modify the motivational effects of nicotine directly infused into the pVTA as suggested by our observations on neuronal activation. We submitted control and AB mice to an intra-VTA SA task (**Table S3** for statistics). Injection sites were located in the pVTA (**Fig.3A**). We previously established that nicotine elicits robust intra-VTA SA behavior at the relatively low dose of 100 ng (salt)/50 nL injection [37,38] which decreases in a dose-dependent manner when high doses are used [23]. In a first experiment, we submitted control and AB mice to very low and increasing doses of nicotine (**Fig.3B**). Neither control nor AB mice self-administered nicotine at the doses of 2 and 10 ng. Yet, when the dose was increased to 50 ng, AB mice started to show SA behavior, in contrast to control mice [sessions 16-18: $F(group)_{1,15} = 6.63$, $p = 0.021$]. In a second experiment, we directly submitted another group of control and AB mice to the 50 ng dose (**Fig.3C**). Contrary to the first experiment, we did not observe significant differences between groups at this dose, suggesting that prior exposure to very low nicotine doses and/or longer AB exposure may be important for enhanced nicotine reward

sensitivity in AB animals. Remarkably, when the dose of nicotine was increased to 500 ng, AB mice developed and maintained SA behavior while control mice avoided nicotine injections [sessions 5-10: $F(group)_{1,18} = 9.239$, $p = 0.007$]. We next switched treatments between groups: we ceased the AB regimen in AB mice for 26 days, a delay sufficient for at least partial gut microbiota restoration [39,40] **(Fig. S3)**, and started exposing control mice to ABs eight days before testing both groups again for nicotine SA at the 500 ng/50 nL dose. Strikingly, mice previously treated with ABs no longer displayed SA behavior at this dose, while mice newly treated with ABs no longer avoided nicotine injections, the number of nicotine self-injections being now higher in the latter [sessions 13-16: $F(group)_{1,18} = 4.479$, $p = 0.048$; sessions 1-16: $F(sessionXgroup)_{15,270} = 5.698$, $p < 0.0001$]. AB-induced global alterations in exploratory behavior in the Y-maze are unlikely to account for the group differences in nicotine SA as there were no differences between groups in the percentage of alternation (**Fig.S4A)** or in the choice latencies that progressively decreased over training sessions (**Fig.S4B-C)**. There were also no differences in the number of self-injections (5,0±-0,1 and 4,6±0,7 (mean±SEM) in control (n=5) and AB mice (n=5) respectively) nor in the percentage of alternation (**Fig.S4A)** in independent groups having access to aCSF only for nine sessions, although choice latencies were increased in AB mice as compared to controls (**Fig.S4B-C)**. These results show that gut microbiota depletion modifies the balance between nicotine's rewarding and aversive effects. Alterations in DA neuron density have been reported after gut microbiota disruptions [41,42]. Here we observed no differences in the number of TH^+ cells between groups (**Fig.3D**, **Table S3**), indicating that the change in sensitivity to nicotine observed in AB mice does not result from altered DA neuron density. The 2D surface of the VTA was not different either between groups (aVTA: 0.299±0.028 and 0.306±0.026 mm2; pVTA: 0.320±0.021 and 0.358±0.024 mm2; in control and AB mice, respectively, **table S3**).

Gut microbiota depletion does not impact nicotine withdrawal

We next examined whether gut microbiota may also contribute to nicotine withdrawal syndrome (**Table S3** for statistics). Control and AB mice were chronically exposed to either nicotine (10 mg/kg/day) or to NaCl, for four weeks. We precipitated withdrawal by administering the nicotinic

receptor antagonist mecamylamine (2mg/kg, IP) [43-46]. We observed no effects of chronic nicotine, ABs, or the combination of both, on anxiety-like behaviors in the dark light box in basal conditions (**Fig.3E-G**). However, anxiety-like behaviors were increased during withdrawal, independently of AB exposure (**Fig.3H-J**). In fact, while the % of time spent in the light side was not altered, there was a significant i) decrease in the number of transitions between both sides [$F(\text{NIC treatment})_{1,51} = 13.34$, $p < 0.0001$] and ii) increase in the latency to first entry into the light side after mecamylamine administration [$F(\text{NIC treatment})_{1,51} = 4.10$, $p = 0.048$], in a similar way in both groups exposed to nicotine as compared to non-exposed mice. AB mice showed a higher basal score of somatic signs than controls [$F(\text{AB treatment})_{1,51} = 41.75$, $p < 0.0001$] (**Fig.3K-L**), which was decreased by nicotine [$F(\text{NIC treatment})_{1,51} = 16.33$, $p = 0.0002$; $F(\text{ABXNIC})_{1,51} = 12.23$, $p = 0.001$] (**Fig.3K**) and the somatic score was enhanced in response to mecamylamine in a similar way in both groups exposed to nicotine [$F(\text{AB treatment})_{1,51} = 5.12$, $p=0.028$; $F(\text{NIC treatment})_{1,51} = 12.51$, $p = 0.0009$] (**Fig.3L**). Thus, contrary to nicotine reward, gut microbiota depletion does not influence these aspects of nicotine withdrawal in our experimental conditions.

Gut microbiota depletion increases astrocyte density in the pVTA and PSD-95 in VTA non-DA neurons without altering GLT1 density

Glial cells are important regulators of the synaptic changes driven by addictive drugs in the mesolimbic system [17,47]. Astrocytes shape DA activity [17,47] while gut bacteria modulate astrocyte activity via microbial metabolites [16,48]. We next assessed whether gut microbiota depletion may affect astrocyte function within the mesolimbic system (**Table S4** for statistics). Interestingly, after ten days of AB exposure, mice expressed significantly higher levels of $GFAP^+$ astrocytes selectively in the pVTA [$F(\text{area})_{1,13} = 11.42$, $p = 0.0049$; $F(\text{groupXarea})_{1,13} = 12.11$, $p = 0.0041$] (**Fig.4A-C**). Levels of $GFAP^+$ astrocytes were also significantly higher in the pVTA compared to the aVTA in AB mice only (**Fig.4B**). One key function of astrocytes is the clearance of glutamate from the synaptic cleft for neuronal excitability modulation [49]. This occurs primarily through the glutamate transporter GLT1 expressed exclusively on astrocytes [50], proposed as a therapeutic target for drug addiction [51]. Blockade of GLT1 enhances DA neuron excitability

[52,53]. Despite the higher density of pVTA GFAP$^+$ astrocytes in AB mice, GLT1 density was not modified neither in the aVTA nor in the pVTA (**Fig.4D-E**). Yet, GLT1 density was higher in the aVTA compared to the pVTA independently of AB treatment [$F(area)_{1,9}$ = 9.98, p = 0.012] (**Fig.4E**). To obtain further insights into how neuron excitability may be altered in the VTA in conditions of gut microbiota depletion, we next measured the levels of the post-synaptic density protein PSD-95, a scaffolding molecule enriched at glutamatergic synapses that contributes to the regulation of synaptic strength [54] (**Fig.4F-I**, **Table S4**). As for GLT1, we found that total PSD-95 density was higher in the aVTA than in the pVTA [$F(area)_{1,9}$ = 58.53, p < 0.0001]. Moreover, total PSD-95 density was globally higher in the VTA of AB mice compared to controls [$F(group)_{1,14}$ = 5.22, p = 0.038] (**Fig.4G**). This effect concerned only non-DA neurons: while there were no group nor sub-region differences in PSD-95 density specifically on DA neurons (**Fig.4H**), such differences were observed again when quantifying PSD-95 density in the part of the VTA where there were no DA neurons [$F(group)_{1,14}$ = 7.34, p = 0.017; $F(area)_{1,9}$ = 81.57, p < 0.0001] (**Fig.4I**).

Distinct microglial sub-populations exist in the aVTA and pVTA whose distribution is re-organized in conditions of gut microbiota depletion

Microglia are also important regulators of the synaptic changes driven by addictive drugs [17,55]. Microglial heterogeneity and response to dysbiosis has never been described within the VTA although microglia is overrepresented in midbrain DA pathways [56]. We performed an automated and comprehensive microglial morphology analysis as we previously described [28], in both the aVTA and pVTA of mice treated with AB for ten days. Microglia were visualized with antibodies against Iba1 [28] **(Fig.5A).** Fluorescence intensity of each cell was measured for quality control, with no differences between control and AB mice (**Tables S5-6**). We observed no differences between groups in the density, body area (BA), roundness, total process length and maximum process length (MaxL) for both ramified and amoeboid microglia (**Tables S5-6**). For ramified cells, there were no differences between groups in the number of ramifications and segments **(Table S5)**. We further calculated a complexity score (CS) derived from the total number of segments and the covered environment area (CEA), which represents the 2D total surface covered by

ramifications **(Fig.5A)**. Both CS and CEA were similar between groups in the aVTA and pVTA **(Table S5)**.

In a second step, we aimed at better capturing the variability in microglial phenotypes that may be heterogeneous amongst VTA sub-regions and in response to gut microbiota depletion. We first performed a PCA on the main parameters BA, CS, CEA, and MaxL. CS and MaxL correlated in both the aVTA (r_s=0.9, $p<0.0001$) and pVTA (r_s=0.88, $p<0.0001$). We thus performed a clustering analysis considering the parameters CS/CEA/BA or CEA/BA/MaxL to identify distinct subpopulations based on high (+) or low (-) values for each parameter (**Table S7** for statistics). An example of each subpopulation identified is shown in **Fig. 5B**. For the aVTA, CS/CEA/BA k-means clustering identified four subpopulations (**Fig.5C**, **Fig.S5A**). Importantly, the proportion of $CS^-/CEA^+/BA^-$ microglia was increased while that of $CS^+/CEA^-/BA^-$ was decreased in AB mice. By contrast, the proportions of $CS^-/CEA^-/BA^+$ and $CS^-/CEA^-/BA^-$, which were the most represented subpopulations in the aVTA, were not changed. When considering CEA/BA/MaxL in the aVTA, we identified four subpopulations (**Fig.5D, Fig.S5B**). Their distribution was also significantly different between groups with a larger proportion of the overall less represented subpopulation $CEA^+/BA^+/MaxL^-$ in AB mice. In the pVTA, CS/CEA/BA clustering identified four subpopulations (**Fig.5E**, **Fig.S5C**) whose distribution did not vary between groups. Finally, when considering CEA/BA/MaxL in the pVTA, we identified five subpopulations (**Fig.5F**, **Fig.S5D**) amongst which $CEA^-/BA^-/MaxL^-$ microglia was the most represented in AB mice and whose proportion was increased compared to controls, in which $CEA^-/BA^+/MaxL^-$ microglia was the most represented. Moreover, the proportion of $CEA^-/BA^+/MaxL^+$ microglia was decreased in AB mice. Thus, cluster analysis revealed the existence of distinct microglia subpopulations in the different VTA sub-regions. Moreover, subpopulations identified on the basis of the morphological features CS/CEA/BA in the aVTA and CEA/BA/MaxL in both the aVTA and the pVTA were re-organized in response to gut microbiota depletion.

Discussion

Gut microbiota modulation of nicotine-evoked activation of the mesolimbic system and motivational effects

Although the intake of several addictive substances is associated with dysbiosis [4,57,58], very little is known about the influence of gut microbes on the mesolimbic system and its responsiveness to drugs. Here we demonstrate an enhancement of nicotine-induced activation of the mesolimbic system after gut microbiota depletion. The pVTA is the preferential substrate for drug-rewarding effects [8,10,31,59] and preferentially projects to the medial part of the NAcbS. In accordance with this, we found a selective activation of the pVTA and the NAcbS in response to a rewarding dose of nicotine [31,60,61], as well as the IPN that is involved in nicotine avoidance [35,62]. Nicotine motivational effects balance between reward and aversion and nicotine reward is usually observed at a narrow range of doses in animal models, with variability depending on experimental conditions [61,63,64]. Importantly, the lack of microbiota enhanced nicotine effects selectively in the pVTA and the NAcbS, indicating a unique link between gut bacteria and the mesolimbic system in the mediation of nicotine effects.

The AB cocktail we used is a mixture of absorbable and non-absorbable compounds previously validated for gut microbiota depletion in mice [21]. Absorbable ABs show a broader-spectrum action but may have systemic effects. We saw AB-induced enhancement of nicotine activation of the mesolimbic system only after oral exposure, which supports the idea that AB action specifically on bacteria within the digestive tract mediated brain and behavioral alterations as previously observed [13,22]. While ABs deplete microbial populations in mice which were normally colonized since birth thereby preventing impairments in development and early immune education, GF mice exhibit a complete absence of microbes without the risk of off-target effects [65]. Here we have replicated the effects observed in AB-treated SPF mice in GF mice thereby strengthening the validity of our observations.

We further observed that DA neuron sensitivity to nicotine was increased in the pVTA after gut microbiota depletion as exemplified by a decreased threshold dose for firing. This was completed

by the observation that AB mice manifested nicotine appetence at low and high doses that were inefficient and aversive, respectively, in control mice in a procedure of intra-VTA SA. VTA DA neurons have been involved in both rewarding and aversive properties of nicotine, which recruit discrete DA sub-circuits within the mesolimbic system [66-68]. While the rewarding actions of nicotine are crucial in establishing smoking habits, nicotine's aversive effects are thought to protect against transitioning to regular tobacco use [66,69]. By altering the balance between nicotine reward and aversion, gut dysbiosis may represent an underestimated risk factor for tobacco use disorder.

Gut microbiota modulation of astrocytes within the pVTA

Several mechanisms may connect the gut microbiota to VTA DA neurons including bacterial production of short chain fatty acids [70-72], gut peptides [15,57] or the vagus nerve [12,73]. Brain glial cells have also emerged as an important player in gut-brain interactions [16]. Astrocytes integrate information from adjacent cells to modulate neural excitability including VTA synaptic changes driven by addictive drugs [47,55]. Here we observed an increase in astrocyte density specifically in the pVTA in response to gut microbiota depletion. Gut microbes metabolize dietary tryptophan to produce natural ligands of astrocyte aryl hydrocarbon receptors, thereby regulating astrocyte activity [16] that, in turn, modulates drug seeking [17]. The increase in pVTA astrocyte density may be involved in the alteration of nicotine motivational effects associated with gut microbiota depletion, although we have not tested yet such a causal link. Astrocytes modulate synaptic function by controlling glutamate levels notably through the glutamate transporter GLT1 also involved in drug seeking [17,51,74,75]. Here, despite increased pVTA astrocyte density, we did not observe modifications in GLT1 levels after gut microbiota depletion, maybe due to compensatory mechanisms [76]. GLT1 modulation is associated with glutamate activation of extrasynaptic NMDA receptors (NMDARs), critical for drug-induced plasticity [77]. Here we observed increased levels of PDS-95, which stabilizes NMDAR expression, selectively in VTA non-DA neurons in response to gut microbiota depletion. GLT1 can form protein complexes with PSD-95 and NMDARs, an interaction thought to contribute to GLT1 regulation [78]. Further work is

needed to unravel the interplay between astrocytes and glutamatergic post-synaptic signalling in non-DA neurons in conditions of gut dysbiosis, and how this may eventually tune the response of DA neurons to drugs. We also found that both GLT1 and PSD-95 levels were lower in the pVTA as compared to the aVTA. This may be linked to the relatively higher abundance of glutamatergic neurons in the aVTA [59,79].

Identification of region-specific microglial sub-populations within the VTA and their modulation by gut microbiota

Recent studies established that the gut microbiome influences microglia function [19-21]. However, the mesolimbic system was not described in these studies. Microglia produce a variety of factors that modulate DA neurons [17,80]. VTA microglia show specific anatomical features, lysosome content and transcriptome compared to other basal ganglia nuclei [81] and changes in microglia may be a driving factor in the development of drug addiction [17]. Here we identified for the first time several microglia sub-populations in the VTA that differ between its anterior and posterior parts. Importantly, we found that these sub-populations are re-organized following gut microbiota depletion**.** Microglial cells were generally considered either in a 'resting' or 'activated' state mainly based on soma size and degree of ramification. More recently, the co-existence of multifaceted sub-populations and intermediate states of microglia has been proposed [28,82,83], as further supported by our present data. Separate analysis of morphological parameters did not reveal major changes between groups. However, we identified region-specific redistribution of sub-populations based on several main morphological features. Our data revealed the cohesive role of the total surface covered (CEA) by the cell, its body area (BA) and maximum ramification length (MaxL) in the microglial response of the VTA to gut microbiota depletion. We further identified a concerted implication of the cell ramification complexity (CS), CEA and BA in the microglial response of the aVTA, not of the pVTA, to gut microbiota depletion, suggesting the recruitment of distinct microglial functions in the different VTA sub-regions following physiological changes. The CS and CEA indices were previously shown as relevant parameters to identify microglial sub-populations in the

prefrontal cortex in response to neuroinflammation when they were considered together but not separately [28,84]. Taken together, these findings support the relevance of clustering analyses to capture microglial heterogeneity. Additional research is needed to decipher how gut dysbiosis is linked to these region-specific changes in microglia and how these changes may modify DA neurons' sensitivity to stimuli such as nicotine.

In conclusion, the gut bacteria act as modulators of nicotine action on the mesolimbic system and influence its motivational effects. They also regulate post-synaptic density protein levels and the glial cells within the mesolimbic system, the latter in a region-dependent manner. While the present study shows increased astrocyte density and alterations in the distribution of microglial sub-populations within the VTA in response to gut microbiota depletion, whether and how these effects are linked to altered function of these cells and production of inflammatory mediators or other metabolites susceptible to modulate synaptic activity and behavior remains to be identified. These aspects will be important to be considered in future studies with the objective of understanding the putative cause-effect relationship between gut bacteria influence on VTA glial cells and nicotine motivational effects that was not examined here. The use of psychobiotics has been proposed as a novel therapeutic strategy for brain disorders [85], while the brain immune system is a promising target for addiction therapeutics [86]. The use of probiotics with glia modulation properties may be of strong interest for treating drug-, and especially nicotine-addiction. Only male mice were used in the present study while nicotine addiction affect men and women differently [87]. Moreover, recent evidence has shown differential alterations in the gut-brain-axis between female and male rodents after nicotine exposure [88] and in the context of alcohol or opioid addiction [89,90], which supports the importance of examining sex specificities in future investigations into that matter.

Author Contributions

M.B., A.D., V.D., B.F., F.M., U.M designed research; M.B., C.C., V.D., A.L., F.M., A.R., L.R., S.T., L.T., and F.T. performed research; F.D.C. contributed new analytic tools; M.B., C.C., A.D., V.D.,

A.L., F.M., A.R., L.R., S.T., L.T., and F.T. analyzed data; M.B. wrote the original draft of the paper. All co-authors read, reviewed, edited and approved the final manuscript.

Funding

We thank the Biomics and gnotobiology plateforms and animal facilities (Institut Pasteur, Paris). This work was supported by the Institut Pasteur, Paris (GPF Microbes and Brain, project “µBIOTADDICT”). UtechS PBI/C2RT is part of the France BioImaging infrastructure supported by the French National Research Agency (ANR-10-INSB-04-01, “Investments for the future”) and is supported by Conseil de la Region Ile-de-France (Domaine d’Intérêt Majeur DIM1HEALTH) and by Fondation Française pour la Recherche Médicale (Programme Grands Equipements).

Conflict of Interest

The authors have nothing to disclose.

References

1 Rooks MG, Garrett WS. Gut microbiota, metabolites and host immunity. Nat Rev Immunol. 2016;16(6):341-52.

2 Kelly JR, Minuto C, Cryan JF, Clarke G, Dinan TG. Cross Talk: The Microbiota and Neurodevelopmental Disorders. Front Neurosci. 2017;11:490.

3 Foster JA, Rinaman L, Cryan JF. Stress & the gut-brain axis: Regulation by the microbiome. Neurobiol Stress. 2017;7:124-36.

4 Meckel KR, Kiraly DD. A potential role for the gut microbiome in substance use disorders. Psychopharmacology 2019;236(5):1513-30.

5 Le Foll B, Piper ME, Fowler CD, Tonstad S, Bierut L, Lu L, et al. Tobacco and nicotine use. Nat Rev Dis Primers. 2022;8(1):19.

6 Prochaska JJ, Benowitz NL. Current advances in research in treatment and recovery: Nicotine addiction. Sci Adv. 2019;5(10):eaay9763.

7 Dome P, Lazary J, Kalapos MP, Rihmer Z. Smoking, nicotine and neuropsychiatric disorders. Neurosci Biobehav Rev. 2010;34(3):295-342.

8 Ikemoto S. Dopamine reward circuitry: two projection systems from the ventral midbrain to the nucleus accumbens-olfactory tubercle complex. Brain Res Rev. 2007;56(1):27-78.

9 Di Chiara G, Bassareo V. Reward system and addiction: what dopamine does and doesn't do. Curr Opin Pharmacol. 2007;7(1):69-76.

10 Ikemoto S, Bonci A. Neurocircuitry of drug reward. Neuropharmacology. 2014;76 Pt B:329-41.

11 Buffington SA, Di Prisco GV, Auchtung TA, Ajami NJ, Petrosino JF, Costa-Mattioli M. Microbial Reconstitution Reverses Maternal Diet-Induced Social and Synaptic Deficits in Offspring. Cell. 2016;165(7):1762-75.

12 Sgritta M, Dooling SW, Buffington SA, Momin EN, Francis MB, Britton RA, et al. Mechanisms Underlying Microbial-Mediated Changes in Social Behavior in Mouse Models of Autism Spectrum Disorder. Neuron. 2019;101(2):246-59 e6.

13 Kiraly DD, Walker DM, Calipari ES, Labonte B, Issler O, Pena CJ, et al. Alterations of the Host Microbiome Affect Behavioral Responses to Cocaine. Sci Rep. 2016;6:35455.

14 Lee K, Vuong HE, Nusbaum DJ, Hsiao EY, Evans CJ, Taylor AMW. The gut microbiota mediates reward and sensory responses associated with regimen-selective morphine dependence. Neuropsychopharmacology. 2018;43(13):2606-14.

15 Engel JA, Jerlhag E. Role of appetite-regulating peptides in the pathophysiology of addiction: implications for pharmacotherapy. CNS Drugs. 2014;28(10):875-86.

16 Fung TC, Olson CA, Hsiao EY. Interactions between the microbiota, immune and nervous systems in health and disease. Nat Neurosci. 2017;20(2):145-55.

17 Linker KE, Cross SJ, Leslie FM. Glial mechanisms underlying substance use disorders. Eur J Neurosci. 2019;50(3):2574-89.

18 Anbalagan S. Endocrine cross-talk between the gut microbiome and glial cells in development and disease. J Neuroendocrinol. 2021;33(5):e12924.

19 Mossad O, Erny D. The microbiota-microglia axis in central nervous system disorders. Brain Pathol. 2020;30(6):1159-77.

20 Erny D, Hrabe de Angelis AL, Jaitin D, Wieghofer P, Staszewski O, David E, et al. Host microbiota constantly control maturation and function of microglia in the CNS. Nat Neurosci. 2015;18(7):965-77.

21 Thion MS, Low D, Silvin A, Chen J, Grisel P, Schulte-Schrepping J, et al. Microbiome Influences Prenatal and Adult Microglia in a Sex-Specific Manner. Cell. 2018;172(3):500-16 e16.

22 Bercik P, Denou E, Collins J, Jackson W, Lu J, Jury J, et al. The intestinal microbiota affect central levels of brain-derived neurotropic factor and behavior in mice. Gastroenterology. 2011;141(2):599-609, 09 e1-3.

23 Husson M, Harrington L, Tochon L, Cho Y, Ibanez-Tallon I, Maskos U, et al. beta4-Nicotinic Receptors Are Critically Involved in Reward-Related Behaviors and Self-Regulation of Nicotine Reinforcement. J Neurosci. 2020;40(17):3465-77.

24 Maskos U, Molles BE, Pons S, Besson M, Guiard BP, Guilloux JP, et al. Nicotine reinforcement and cognition restored by targeted expression of nicotinic receptors. Nature. 2005;436(7047):103-7.

25 Tolu S, Eddine R, Marti F, David V, Graupner M, Pons S, et al. Co-activation of VTA DA and GABA neurons mediates nicotine reinforcement. Mol Psychiatry. 2013;18(3):382-93.

26 Besson M, Granon S, Mameli-Engvall M, Cloez-Tayarani I, Maubourguet N, Cormier A, et al. Long-term effects of chronic nicotine exposure on brain nicotinic receptors. Proc Natl Acad Sci U S A. 2007;104(19):8155-60.

27 Saravia R, Flores A, Plaza-Zabala A, Busquets-Garcia A, Pastor A, de la Torre R, et al. CB1 Cannabinoid Receptors Mediate Cognitive Deficits and Structural Plasticity Changes During Nicotine Withdrawal. Biol Psychiatry. 2017;81(7):625-34.

28 Verdonk F, Roux P, Flamant P, Fiette L, Bozza FA, Simard S, et al. Phenotypic clustering: a novel method for microglial morphology analysis. J Neuroinflammation. 2016;13(1):153.

29 Ge X, Ding C, Zhao W, Xu L, Tian H, Gong J, et al. Antibiotics-induced depletion of mice microbiota induces changes in host serotonin biosynthesis and intestinal motility. J Transl Med. 2017;15(1):13.

30 Kovacs KJ. c-Fos as a transcription factor: a stressful (re)view from a functional map. Neurochem Int. 1998;33(4):287-97.

31 Zhao-Shea R, Liu L, Soll LG, Improgo MR, Meyers EE, McIntosh JM, et al. Nicotine-mediated activation of dopaminergic neurons in distinct regions of the ventral tegmental area. Neuropsychopharmacology. 2011;36(5):1021-32.

32 Subramaniyan M, Dani JA. Dopaminergic and cholinergic learning mechanisms in nicotine addiction. Ann N Y Acad Sci. 2015;1349:46-63.

33 Ables JL, Gorlich A, Antolin-Fontes B, Wang C, Lipford SM, Riad MH, et al. Retrograde inhibition by a specific subset of interpeduncular alpha5 nicotinic neurons regulates nicotine preference. Proc Natl Acad Sci U S A. 2017;114(49):13012-17.

34 Harrington L, Vinals X, Herrera-Solis A, Flores A, Morel C, Tolu S, et al. Role of beta4* Nicotinic Acetylcholine Receptors in the Habenulo-Interpeduncular Pathway in Nicotine Reinforcement in Mice. Neuropsychopharmacology. 2016;41(7):1790-802.

35 Morton G, Nasirova N, Sparks DW, Brodsky M, Sivakumaran S, Lambe EK, et al. Chrna5-Expressing Neurons in the Interpeduncular Nucleus Mediate Aversion Primed by Prior Stimulation or Nicotine Exposure. J Neurosci. 2018;38(31):6900-20.

36 Forget B, Scholze P, Langa F, Morel C, Pons S, Mondoloni S, et al. A Human Polymorphism in CHRNA5 Is Linked to Relapse to Nicotine Seeking in Transgenic Rats. Current biology. 2018;28(20):3244-53.e7.

37 Besson M, David V, Baudonnat M, Cazala P, Guilloux JP, Reperant C, et al. Alpha7-nicotinic receptors modulate nicotine-induced reinforcement and extracellular dopamine outflow in the mesolimbic system in mice. Psychopharmacology 2012;220(1):1-14.

38 David V, Besson M, Changeux JP, Granon S, Cazala P. Reinforcing effects of nicotine microinjections into the ventral tegmental area of mice: dependence on cholinergic nicotinic and dopaminergic D1 receptors. Neuropharmacology. 2006;50(8):1030-40.

39 Suez J, Zmora N, Zilberman-Schapira G, Mor U, Dori-Bachash M, Bashiardes S, et al. Post-Antibiotic Gut Mucosal Microbiome Reconstitution Is Impaired by Probiotics and Improved by Autologous FMT. Cell. 2018;174(6):1406-23 e16.

40 Tirelle P, Breton J, Riou G, Dechelotte P, Coeffier M, Ribet D. Comparison of different modes of antibiotic delivery on gut microbiota depletion efficiency and body composition in mouse. BMC Microbiol. 2020;20(1):340.

41 Choi JG, Kim N, Ju IG, Eo H, Lim SM, Jang SE, et al. Oral administration of Proteus mirabilis damages dopaminergic neurons and motor functions in mice. Sci Rep. 2018;8(1):1275.

42 Koutzoumis DN, Vergara M, Pino J, Buddendorff J, Khoshbouei H, Mandel RJ, et al. Alterations of the gut microbiota with antibiotics protects dopamine neuron loss and improve motor deficits in a pharmacological rodent model of Parkinson's disease. Exp Neurol. 2020;325:113159.

43 Damaj MI, Kao W, Martin BR. Characterization of spontaneous and precipitated nicotine withdrawal in the mouse. J Pharmacol Exp Ther. 2003;307(2):526-34.

44 Hughes JR. Effects of abstinence from tobacco: valid symptoms and time course. Nicotine Tob Res. 2007;9(3):315-27.

45 Stoker AK, Semenova S, Markou A. Affective and somatic aspects of spontaneous and precipitated nicotine withdrawal in C57BL/6J and BALB/cByJ mice. Neuropharmacology. 2008;54(8):1223-32.

46 Besson M, David V, Suarez S, Cormier A, Cazala P, Changeux JP, et al. Genetic dissociation of two behaviors associated with nicotine addiction: beta-2 containing nicotinic

receptors are involved in nicotine reinforcement but not in withdrawal syndrome. Psychopharmacology 2006;187(2):189-99.

47 Xin W, Edwards N, Bonci A. VTA dopamine neuron plasticity - the unusual suspects. Eur J Neurosci. 2016;44(12):2975-83.

48 Rothhammer V, Mascanfroni ID, Bunse L, Takenaka MC, Kenison JE, Mayo L, et al. Type I interferons and microbial metabolites of tryptophan modulate astrocyte activity and central nervous system inflammation via the aryl hydrocarbon receptor. Nat Med. 2016;22(6):586-97.

49 Bachtell RK, Jones JD, Heinzerling KG, Beardsley PM, Comer SD. Glial and neuroinflammatory targets for treating substance use disorders. Drug Alcohol Depend. 2017;180:156-70.

50 Williams SM, Sullivan RK, Scott HL, Finkelstein DI, Colditz PB, Lingwood BE, et al. Glial glutamate transporter expression patterns in brains from multiple mammalian species. Glia. 2005;49(4):520-41.

51 Roberts-Wolfe DJ, Kalivas PW. Glutamate Transporter GLT-1 as a Therapeutic Target for Substance Use Disorders. CNS Neurol Disord Drug Targets. 2015;14(6):745-56.

52 Wild AR, Bollands M, Morris PG, Jones S. Mechanisms regulating spill-over of synaptic glutamate to extrasynaptic NMDA receptors in mouse substantia nigra dopaminergic neurons. Eur J Neurosci. 2015;42(9):2633-43.

53 Hardaway JA, Sturgeon SM, Snarrenberg CL, Li Z, Xu XZ, Bermingham DP, et al. Glial Expression of the Caenorhabditis elegans Gene swip-10 Supports Glutamate Dependent Control of Extrasynaptic Dopamine Signaling. J Neurosci. 2015;35(25):9409-23.

54 Gerrow K, El-Husseini A. Cell adhesion molecules at the synapse. Front Biosci. 2006;11:2400-19.

55 Stellwagen D, Kemp GM, Valade S, Chambon J. Glial regulation of synaptic function in models of addiction. Curr Opin Neurobiol. 2019;57:179-85.

56 Kim WG, Mohney RP, Wilson B, Jeohn GH, Liu B, Hong JS. Regional difference in susceptibility to lipopolysaccharide-induced neurotoxicity in the rat brain: role of microglia. J Neurosci. 2000;20(16):6309-16.

57 Garcia-Cabrerizo R, Carbia C, O Riordan K, Schellekens H, Cryan JF. Microbiota-gut-brain axis as a regulator of reward processes. J Neurochem. 2020;157(5):1495-524.

58 Lin D, Hutchison KE, Portillo S, Vegara V, Ellingson JM, Liu J, et al. Association between the oral microbiome and brain resting state connectivity in smokers. Neuroimage. 2019;200:121-31.

59 Sanchez-Catalan MJ, Kaufling J, Georges F, Veinante P, Barrot M. The antero-posterior heterogeneity of the ventral tegmental area. Neuroscience. 2014;282:198-216.

60 Tapper AR, McKinney SL, Nashmi R, Schwarz J, Deshpande P, Labarca C, et al. Nicotine activation of alpha4* receptors: sufficient for reward, tolerance, and sensitization. Science. 2004;306(5698):1029-32.

61 Jackson KJ, Walters CL, Miles MF, Martin BR, Damaj MI. Characterization of pharmacological and behavioral differences to nicotine in C57Bl/6 and DBA/2 mice. Neuropharmacology. 2009;57(4):347-55.

62 Elayouby KS, Ishikawa M, Dukes AJ, Smith ACW, Lu Q, Fowler CD, et al. alpha3* Nicotinic acetylcholine receptors in the habenula-interpeduncular nucleus circuit regulate nicotine intake. J Neurosci. 2021;41(8):1779-87.

63 Clemens KJ, Caille S, Cador M. The effects of response operandum and prior food training on intravenous nicotine self-administration in rats. Psychopharmacology 2010;211(1):43-54.

64 Pons S, Fattore L, Cossu G, Tolu S, Porcu E, McIntosh JM, et al. Crucial role of alpha4 and alpha6 nicotinic acetylcholine receptor subunits from ventral tegmental area in systemic nicotine self-administration. J Neurosci. 2008;28(47):12318-27.

65 Kennedy EA, King KY, Baldridge MT. Mouse Microbiota Models: Comparing Germ-Free Mice and Antibiotics Treatment as Tools for Modifying Gut Bacteria. Front Physiol. 2018;9:1534.

66 Wills L, Ables JL, Braunscheidel KM, Caligiuri SPB, Elayouby KS, Fillinger C, et al. Neurobiological Mechanisms of Nicotine Reward and Aversion. Pharmacol Rev. 2022;74(1):271-310.

67 Liu C, Tose AJ, Verharen JPH, Zhu Y, Tang LW, de Jong JW, et al. An inhibitory brainstem input to dopamine neurons encodes nicotine aversion. Neuron. 2022 Aug 2. https://doi.org/10.1016/j.neuron.2022.07.003.

68 Grieder TE, Besson M, Maal-Bared G, Pons S, Maskos U, van der Kooy D. beta2* nAChRs on VTA dopamine and GABA neurons separately mediate nicotine aversion and reward. Proc Natl Acad Sci U S A. 2019;116(51):25968-73.

69 Sartor CE, Lessov-Schlaggar CN, Scherrer JF, Bucholz KK, Madden PA, Pergadia ML, et al. Initial response to cigarettes predicts rate of progression to regular smoking: findings from an offspring-of-twins design. Addict Behav. 2010;35(8):771-8.

70 Nankova BB, Agarwal R, MacFabe DF, La Gamma EF. Enteric bacterial metabolites propionic and butyric acid modulate gene expression, including CREB-dependent catecholaminergic neurotransmission, in PC12 cells--possible relevance to autism spectrum disorders. PLoS One. 2014;9(8):e103740.

71 Shah P, Nankova BB, Parab S, La Gamma EF. Short chain fatty acids induce TH gene expression via ERK-dependent phosphorylation of CREB protein. Brain Res. 2006;1107(1):13-23.

72 El-Ansary AK, Ben Bacha A, Kotb M. Etiology of autistic features: the persisting neurotoxic effects of propionic acid. J Neuroinflammation. 2012;9:74.

73 Han W, Tellez LA, Perkins MH, Perez IO, Qu T, Ferreira J, et al. A Neural Circuit for Gut-Induced Reward. Cell. 2018;175(3):887-88.

74 Fouyssac M, Belin D. Beyond drug-induced alteration of glutamate homeostasis, astrocytes may contribute to dopamine-dependent intrastriatal functional shifts that underlie the development of drug addiction: A working hypothesis. Eur J Neurosci. 2019;50(6):3014-27.

75 Alajaji M, Bowers MS, Knackstedt L, Damaj MI. Effects of the beta-lactam antibiotic ceftriaxone on nicotine withdrawal and nicotine-induced reinstatement of preference in mice. Psychopharmacology 2013;228(3):419-26.

76 Perego C, Vanoni C, Bossi M, Massari S, Basudev H, Longhi R, et al. The GLT-1 and GLAST glutamate transporters are expressed on morphologically distinct astrocytes and regulated by neuronal activity in primary hippocampal cocultures. J Neurochem. 2000;75(3):1076-84.

77 Shen HW, Scofield MD, Boger H, Hensley M, Kalivas PW. Synaptic glutamate spillover due to impaired glutamate uptake mediates heroin relapse. J Neurosci. 2014;34(16):5649-57.

78 Gonzalez-Gonzalez IM, Garcia-Tardon N, Gimenez C, Zafra F. Splice variants of the glutamate transporter GLT1 form hetero-oligomers that interact with PSD-95 and NMDA receptors. J Neurochem. 2009;110(1):264-74.

79 Morales M, Root DH. Glutamate neurons within the midbrain dopamine regions. Neuroscience. 2014;282:60-8.

80 Treadway MT, Cooper JA, Miller AH. Can't or Won't? Immunometabolic Constraints on Dopaminergic Drive. Trends Cogn Sci. 2019;23(5):435-48.

81 De Biase LM, Schuebel KE, Fusfeld ZH, Jair K, Hawes IA, Cimbro R, et al. Local Cues Establish and Maintain Region-Specific Phenotypes of Basal Ganglia Microglia. Neuron. 2017;95(2):341-56 e6.

82 Lynch MA. The multifaceted profile of activated microglia. Mol Neurobiol. 2009;40(2):139-56.

83 Torres-Platas SG, Comeau S, Rachalski A, Bo GD, Cruceanu C, Turecki G, et al. Morphometric characterization of microglial phenotypes in human cerebral cortex. J Neuroinflammation. 2014;11:12.

84 Kongsui R, Johnson SJ, Graham BA, Nilsson M, Walker FR. A combined cumulative threshold spectra and digital reconstruction analysis reveal structural alterations of

microglia within the prefrontal cortex following low-dose LPS administration. Neuroscience. 2015;310:629-40.

85 Del Toro-Barbosa M, Hurtado-Romero A, Garcia-Amezquita LE, Garcia-Cayuela T. Psychobiotics: Mechanisms of Action, Evaluation Methods and Effectiveness in Applications with Food Products. Nutrients. 2020;12(12).

86 Beardsley PM, Hauser KF. Glial modulators as potential treatments of psychostimulant abuse. Adv Pharmacol. 2014;69:1-69.

87 Verplaetse TL, Morris ED, McKee SA, Cosgrove KP. Sex differences in the nicotinic acetylcholine and dopamine receptor systems underlying tobacco smoking addiction. Curr Opin Behav Sci. 2018;23:196-202.

88 Chi L, Mahbub R, Gao B, Bian X, Tu P, Ru H, et al. Nicotine Alters the Gut Microbiome and Metabolites of Gut-Brain Interactions in a Sex-Specific Manner. Chem Res Toxicol. 2017;30(12):2110-19.

89 Pizarro N, Kossatz E, Gonzalez P, Gamero A, Veza E, Fernandez C, et al. Sex-Specific Effects of Synbiotic Exposure in Mice on Addictive-Like Behavioral Alterations Induced by Chronic Alcohol Intake Are Associated With Changes in Specific Gut Bacterial Taxa and Brain Tryptophan Metabolism. Front Nutr. 2021;8:750333.

90 Ren M, Lotfipour S. Dose- and Sex-Dependent Bidirectional Relationship between Intravenous Fentanyl Self-Administration and Gut Microbiota. Microorganisms. 2022;10(6).

Figure legends

Figure 1. Antibiotic-induced or constitutive gut microbiota depletion enhances nicotine-induced activation of the mesolimbic system

See **Table S1** for statistics.

A. Caecum size in control (n=9) and antibiotic-treated (AB) mice (n=8) shown as mean±SEM. Caecum sizes were compared with unpaired Student t-tests. Examples of caeca in one control (*left*) and one AB mouse (*right*). Scale bar: 1 cm.

B. Fecal DNA concentration in control (n=4) and AB mice (n=4) shown as median with interquartile range. Fecal DNA concentrations were analyzed with Mann-Whitney tests.

C. Bar plots of the relative abundance of phyla in control mice (n=4), AB mice (n=4), control mice intraperitoneally (IP) injected with NaCl (IP control, n=8, see **Fig.1L-M**) and mice IP injected with ABs (IP AB, n=8, see **Fig.1L-M)**.

D. Principal coordinate analysis (PCoA) plot of Bray-Curtis distances for bacterial communities in control (1B), AB (1A), IP control (2B) and IP AB (2A) mice. % of the main coordinates represent their relative contribution to sample differences. Distances between sample points represent their level of dissimilarity. Permanova test was performed to analyze the variance using distance matrices.

E-I. Levels of c-Fos expression in control mice and in mice exposed ABs in their drinking water, in response to NaCl or nicotine (0.5mg/kg), in **(E)** the anterior (aVTA) and posterior (pVTA) ventral tegmental area, the nucleus accumbens shell (NAcbS) and core (NAcbC), **(F)** the interpeduncular nucleus (IPN)), **(G)** the dentate gyrus of the hippocampus (DG), **(H)** the cingulate (Cg), prelimbic (PrL) and infralimbic (IL) cortices, and **(I)** the basolateral (BLA), lateral (LA) and central (CeA) nuclei of the amygdala (Control-NaCl, n=4-7; Control-Nic, n=4-7; AB-NaCl, n=4-8; AB-Nic, n=4-8).

J-K Levels of c-Fos expression in mice exposed to IP NaCl injections (control) and in mice exposed to IP AB injections, in response to NaCl or nicotine, in **(J)** the aVTA and pVTA, the NAcbS and

NAcbC (IP Control-NaCl, n=6-7; IP Control-Nic, n=5-8; IP AB-NaCl, n=7-10; IP AB-Nic, n=7-8); and **(K)** the IPN (IP Control-NaCl, n=4; IP Control-Nic, n=3; IP AB-NaCl, n=2; IP AB-Nic, n=3).

(L) Caecum size in IP Control (n=19) and IP AB (n=19) mice and **(M)** fecal DNA concentration in IP Control (n=8) and IP AB (n=8) mice, shown as mean±SEM. Caecum sizes and fecal DNA concentration were compared with unpaired Student t-tests.

N-O. Levels of c-Fos expression in specific pathogen free (SPF) mice and in germ-free (GF) mice in response to NaCl or nicotine, in **(N)** the aVTA and pVTA, the NAcbS and NAcbC, and **(O)** the IPN (SPF-NaCl, n=9-10; SPF-Nic, n=9-10; GF-NaCl, n=8-10; GF-Nic, n=9-10).

Unless otherwise specified, data shown represent the median as the central mark of the box, the 25th and 75th percentiles as the edges of the box, and the most extreme data points that are not considered outliers as the end of the whiskers. Since assumptions for parametric tests were not met for c-Fos expression datasets, Kruskal-Wallis tests were used. Significant main effects were further analyzed using Dunn's tests for multiple comparisons.

Group effects: *p<0.05, **p<0.01, ***p<0.001.

Figure 2. Gut microbiota depletion enhances nicotine-evoked responses of dopaminergic neurons of the posterior ventral tegmental area.

See **Table S2** for statistics.

A. Post-recording identification of neurobiotin-labeled dopaminergic (DA) DA neurons in the ventral tegmental area (VTA) by immunofluorescence (TH = tyrosine hydroxylase, Neurobiotin = streptavidin-AMCA against neurobiotin). All recorded neurons are identified as TH^+ cells.

B. Analysis of the spontaneous activity of posterior VTA (pVTA) DA neurons in control mice (n=18 cells) and in mice exposed to antibiotics (AB mice, n=21 cells). Cumulative distribution of DA neuron firing rates *(left)* and percentage of spikes-within-burst (%SWB) *(right)*. Comparisons of spontaneous activity distribution were performed with Kolmogorov-Smirnov tests.

C. Recording trace of one pVTA DA neuron during intravenous (IV) injection of nicotine (Nic, 30 µg/kg) *(top)*. Example of firing frequency variation induced by NaCl or different doses of nicotine (7.5, 15, 30 and 60 µg/kg) in one DA neuron *(bottom)*.

D. Mean firing frequency variation of pVTA DA neurons induced by nicotine injection (dashed line) in control and AB mice

E. Dose-response curves of maximum of firing variation induced by nicotine in pVTA DA neurons of control (n=18 cells) and AB (n=21 cells) mice. Mean maximum of firing variation induced by NaCl (white dot) is compared to those induced by different doses of nicotine. The dashed lines indicate the thresholds of response at the population level determined by the first dose of nicotine inducing a significant firing variation compared to saline injection. Ratio of active cells are also shown for each dose of nicotine. Comparisons between means of firing variation induced by saline and nicotine were performed using parametric Student's t-tests when parameters followed a normal distribution (Shapiro-Wilk normality test $p>0.05$), or Wilcoxon non-parametric tests when the distribution was skewed. Bonferroni correction was applied for multiple comparisons. For comparison of nicotine responses between groups, data were analyzed by fitting a mixed model using AB-treatment as between-subject factor and nicotine dose as within-subject factor. Ratio of active cells were compared between groups with chi-square tests.

Unless otherwise specified, data shown represent mean±SEM. Nicotine effects: *p<0.05, **p<0.01, ***p<0.001. Group effect: $^{\#}p<0.05$, $^{\#\#}p<0.01$

Figure 3. Gut microbiota depletion modifies nicotine's motivational effects without altering nicotine withdrawal syndrome.

See **Table S3** for statistics.

A. Localization of injection sites on brain coronal sections for all mice used in the intra-ventral tegmental area (VTA) nicotine self-administration experiments, and photomicrograph of a thionine-stained coronal brain section (50 µm) through the cannula track and the injection site within the VTA.

B. Number of intra-VTA injections in control (n=9) and AB mice (n=9) having access to nicotine (2 ng/µL, 10 ng/µL and 50 ng/µL) (experiment 1).

C. Number of intra-VTA injections in control (n=10) and AB mice (n=10) whose treatments were inverted between sessions 10 and 11 (AB regimen was stopped in AB mice for 26 days and control mice were exposed to ABs 8 days before S11), having access to nicotine (50 ng/µL and 500 ng/µL) (experiment 2). Data were analyzed with two-way repeated-measure ANOVAs (group as between-subject and session as within-subject factors).

D. Density of tyrosine hydroxylase positive (TH^+) cells in the anterior (aVTA) and posterior (pVTA) VTA in control (n=5 (aVTA) or 6 (pVTA)) and AB mice (n=6). Since for some animals data for both VTA sub-regions were missing, data were analyzed by fitting a mixed model (rather than by repeated measures ANOVA, which cannot handle missing values), using AB-treatment as between-subject factor and brain area as within-subject factor.

(E) Number of transitions, **(F)** % of time spent in the light side and **(G)** latency to first entry into the light side in the dark-light-box (DLB) in control and AB mice during chronic nicotine. **(H)** Number of transitions, **(I)** % of time spent in the light side and **(J)** latency to first entry into the light side in the DLB in control and AB mice in response to mecamylamine after chronic nicotine (Control-Nic ± MEC, n=14; AB-Nic ± MEC, n=12) or NaCl (Control-NaCl ± MEC, n=15; AB-NaCl ± MEC, n=14). Data were analyzed with two-way ANOVAs (AB- and nicotine-treatment as between-subject factors). Significant main effects were further analyzed using Bonferroni for multiple comparisons post hoc tests.

(K) Number of somatic signs in control and AB mice during chronic nicotine or **(L)** in response to mecamylamine after chronic nicotine (Control-Nic ± MEC, n=14; AB-Nic ± MEC, n=12) or NaCl (Control-NaCl ± MEC, n=15; AB-NaCl ± MEC, n=14). Data were analyzed with two-way ANOVAs (AB- and nicotine-treatment as between-subject factors). Significant main effects were further analyzed using Bonferroni for multiple comparisons post hoc tests.

Data shown represent mean±SEM. AB effects: $^{*}p<0.05$, $^{***}p<0.001$. Nicotine effects: $^{\#}p<0.05$, $^{\#\#\#}p<0.001$.

Figure 4. Gut microbiota depletion increases astrocyte and post-synaptic protein, but not GLT1, density in the ventral tegmental area.

See **Table S4** for statistics.

A. Representative glial fibrillary acidic protein (GFAP) and tyrosine hydroxylase (TH) immunofluorescence (X20) in the posterior ventral tegmental area (pVTA).

B. Density of $GFAP^+$ cells in the anterior VTA (aVTA) and pVTA in control mice (n=11 (aVTA) or 9 (pVTA)) and mice exposed to antibiotics (AB mice (n=11 (aVTA) or 12 (pVTA)).

C. Density of $GFAP^+$ cells in the nucleus accumbens shell (NAcbS) and core (NAcbC) in control (n=6) and AB (n=5) mice.

D. Representative glutamate transporter 1 (GLT1) and TH immunofluorescence (X40) in the aVTA.

E. Density of GLT1 in the aVTA and pVTA in control (n=8 (aVTA) or 9 (pVTA)) and AB (n=8 (aVTA) or 7 (pVTA)) mice.

F. Representative post-synaptic density protein 95 (PSD-95) and TH immunofluorescence (X60) in the pVTA.

(G) Density of PSD-95 in the aVTA and pVTA in control (n=7) and AB (n=6 (aVTA) or 7 (pVTA)) mice; **(H)** in TH^+ area; **(I)** in TH^- area.

Since for some animals data for both VTA sub-regions were missing, data were analyzed by fitting a mixed model using AB-treatment as between-subject factor and brain area as within-subject factor. Sidak's post hoc tests were used for multiple comparisons upon significant main effects. For the NAcb, two-way repeated measures ANOVAs were used. Data shown represent mean±SEM. Group effects: $^*p<0.05$. Area effects: $^{\#}p<0.05$, $^{\#\#\#}p<0.001$.

Figure 5. Distinct microglial sub-populations are present in the anterior and posterior ventral tegmental area, and their distribution is re-organized in conditions of gut microbiota depletion.

See **Table S7** for statistics.

A. Confocal image showing individual microglia based on Iba1 fluorescence in a sub-part of the ventral tegmental area (VTA) after maximum intensity projection *(left)*. Ramification detection with Acapella™ software *(right)*: the cell body detection (body area, BA, green) serves as a starting point to characterize a microglial cell. The complexity score (CS, blue), associated with white arrows showing a secondary and tertiary ramification, and the covered environment area (CEA, orange) are deduced from ramification detection (BA, CS and CEA have been artificially colored for better representation). Scale bar, 50 µm.

B. Representative microglia cells for each subpopulation identified in the anterior and/or posterior VTA through clustering based on CS, CEA and BA *(top)* or CEA, BA and MaxL *(bottom)* characteristics (high (+) or low (-) values). The associated color code is re-used in panels C and D for better visualization. Scale bar, 10µm.

C. Pie charts representing the proportions of each microglial subpopulation based on CS, CEA and BA characteristics (high (+) or low (-) values) in the anterior VTA (Ant VTA), in control (n=386 cells) and AB mice (n=559 cells)

D. Pie charts representing the proportions of each microglial subpopulation based on CEA, BA and MaxL characteristics (high (+) or low (-) values) in the anterior VTA (Ant VTA), in control (n=386 cells) and AB mice (n=559 cells)

E. Pie charts representing the proportions of each microglial subpopulation based on CS, CEA and BA characteristics (high (+) or low (-) values) in the posterior VTA (Post VTA), in control (n=474 cells) and AB mice (n=628 cells).

F. Pie charts representing the proportions of each microglial subpopulation based on CEA, BA and MaxL characteristics (high (+) or low (-) values) in the posterior VTA (Post VTA), in control (n=472 cells) and AB mice (n=625 cells).

A principal component analysis and a k-means clustering method were used for sub-population identification. For each feature and each cluster, a '+' or '–' sign was assigned. The statistics of each cluster (mean and frequency) were used to characterize sub-populations and determine their phenotype. Clustering phenotype distributions were compared between groups with chi-square

tests. Upon significant effects, Z tests were used for proportion comparisons between groups for each cell sub-population.

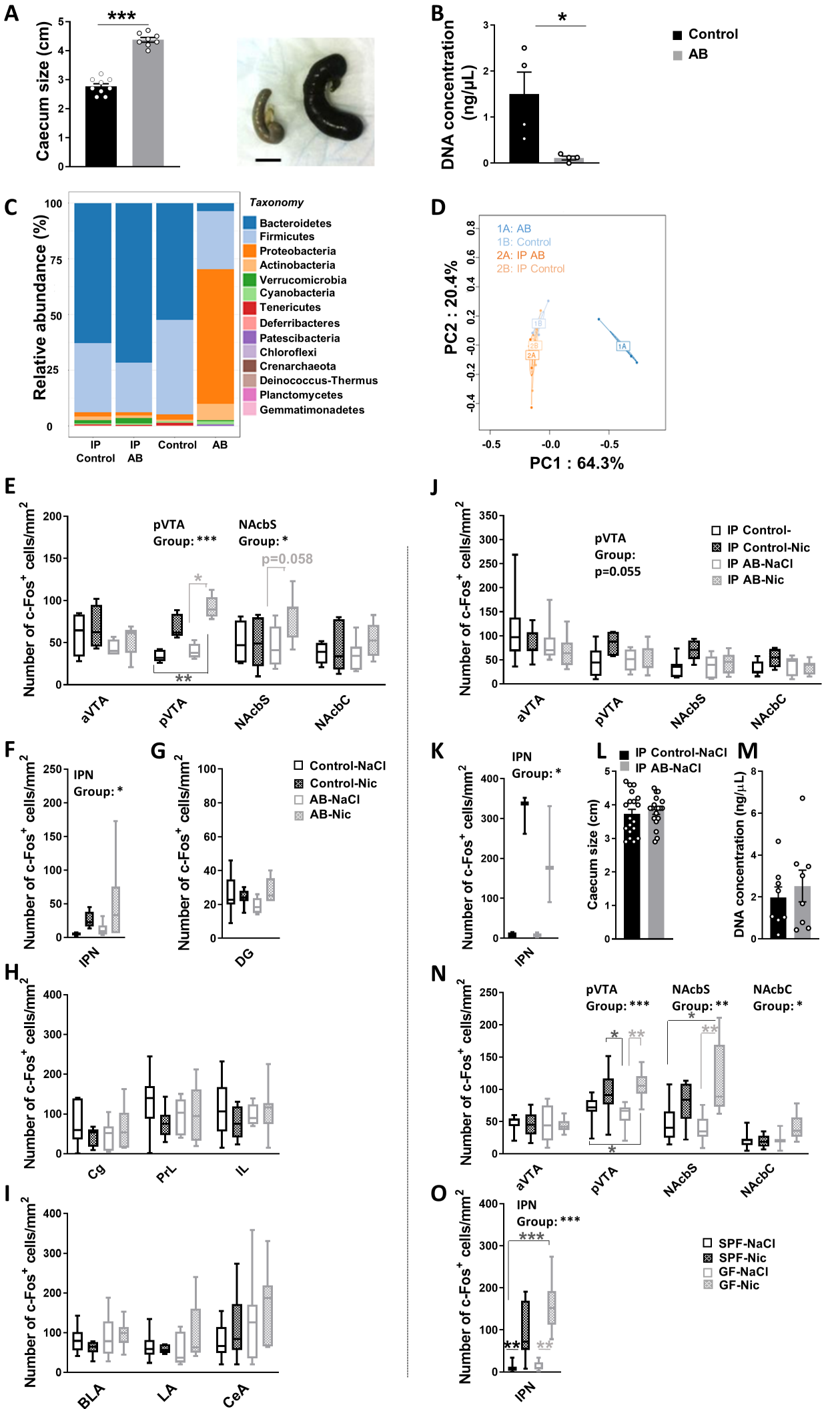
A
***
Caecum size (cm)
B
*
DNA concentration (ng/μL)
Control
AB
C
Taxonomy
Bacteroidetes
Firmicutes
Proteobacteria
Actinobacteria
Verrucomicrobia
Cyanobacteria
Tenericutes
Deferribacteres
Patescibacteria
Chloroflexi
Crenarchaeota
Deinococcus-Thermus
Planctomycetes
Gemmatimonadetes
Relative abundance (%)
IP Control
IP AB
Control
AB
D
1A: AB
1B: Control
2A: IP AB
2B: IP Control
PC2 : 20.4%
PC1 : 64.3%
E
pVTA Group: ***
NAcbS Group: *
p=0.058
Number of c-Fos+ cells/mm2
aVTA
pVTA
NAcbS
NAcbC
J
pVTA Group: p=0.055
IP Control-
IP Control-Nic
IP AB-NaCl
IP AB-Nic
F
IPN Group: *
G
Control-NaCl
Control-Nic
AB-NaCl
AB-Nic
IPN
DG
K
IPN Group: *
L
IP Control-NaCl
IP AB-NaCl
Caecum size (cm)
M
DNA concentration (ng/μL)
H
Cg
PrL
IL
N
pVTA Group: ***
NAcbS Group: **
NAcbC Group: *
I
BLA
LA
CeA
O
IPN Group: ***
SPF-NaCl
SPF-Nic
GF-NaCl
GF-Nic

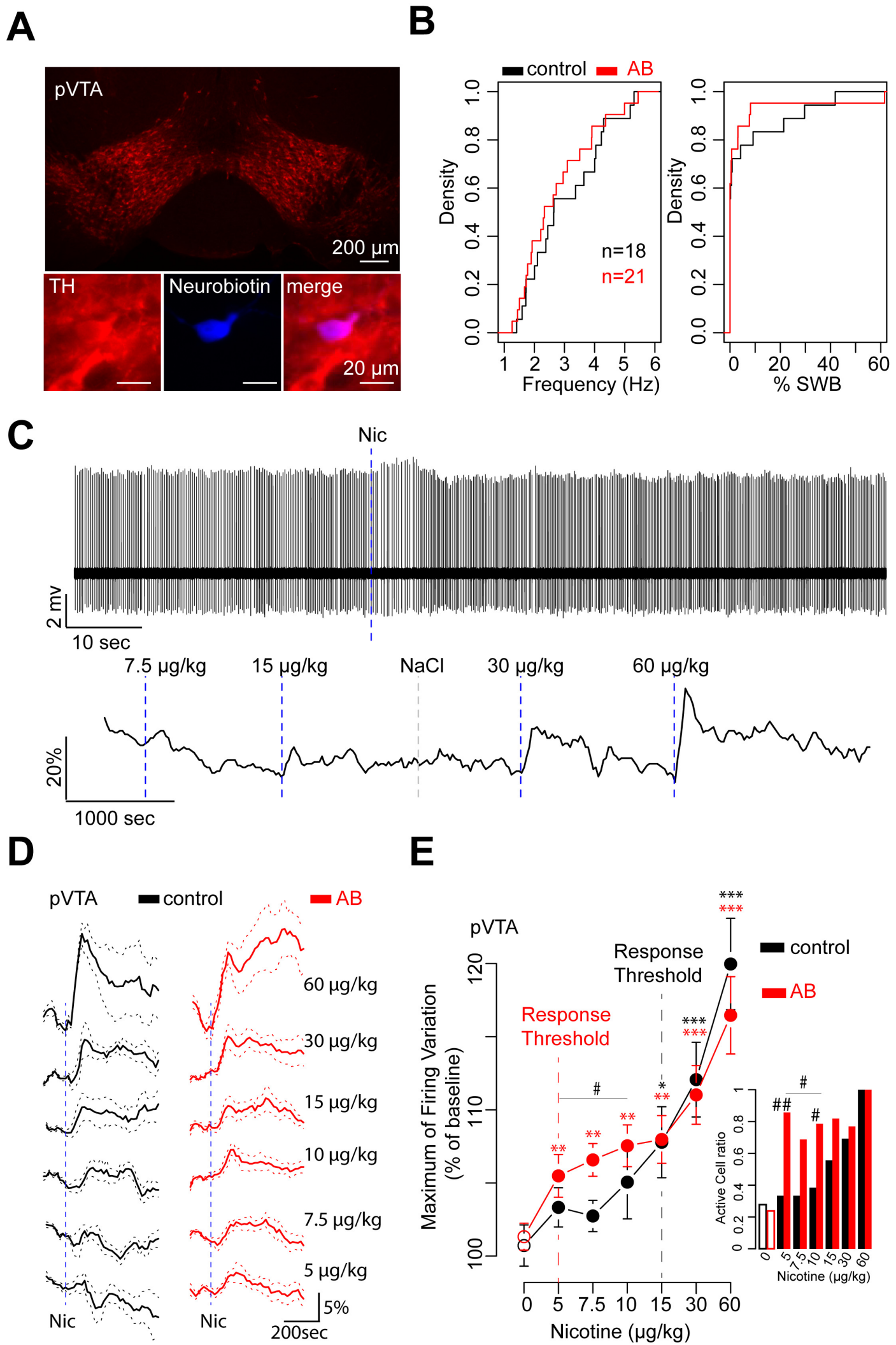
A
pVTA
200 µm
TH
Neurobiotin
merge
20 µm
B
control
AB
Density
n=18
n=21
Frequency (Hz)
% SWB
C
Nic
2 mv
10 sec
7.5 µg/kg
15 µg/kg
NaCl
30 µg/kg
60 µg/kg
20%
1000 sec
D
pVTA
control
AB
60 µg/kg
30 µg/kg
15 µg/kg
10 µg/kg
7.5 µg/kg
5 µg/kg
Nic
Nic
5%
200sec
E
pVTA
Response Threshold
Response Threshold
control
AB
Maximum of Firing Variation (% of baseline)
Nicotine (µg/kg)
Active Cell ratio
Nicotine (µg/kg)

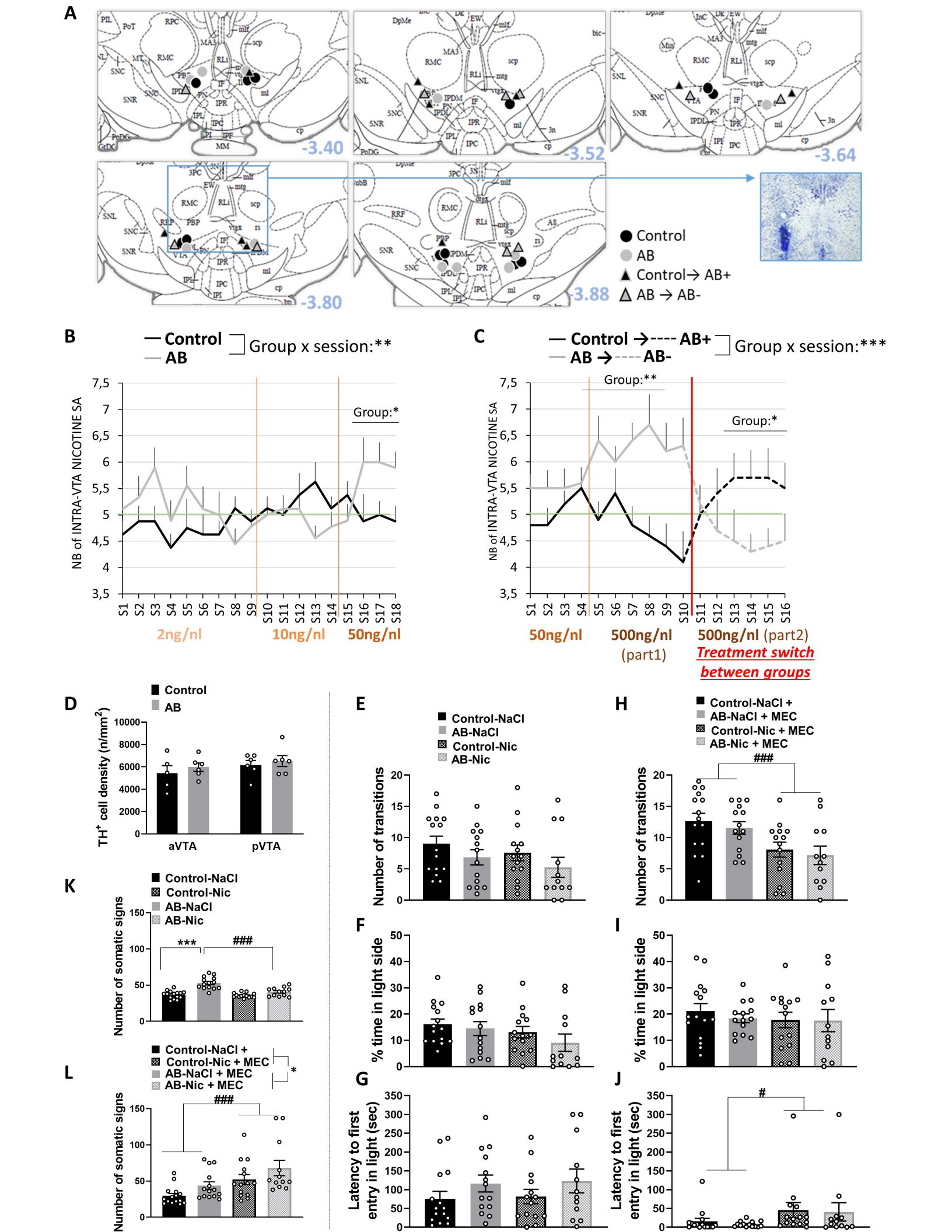
A
-3.40
-3.52
-3.64
-3.80
-3.88
Control
AB
Control→ AB+
AB → AB-
B
Control
AB
Group x session:**
NB of INTRA-VTA NICOTINE SA
Group:*
2ng/nl
10ng/nl
50ng/nl
C
Control →---- AB+
AB →---- AB-
Group x session:***
Group:**
Group:*
50ng/nl
500ng/nl (part1)
500ng/nl (part2)
Treatment switch between groups
D
Control
AB
TH+ cell density (n/mm2)
aVTA
pVTA
E
Control-NaCl
AB-NaCl
Control-Nic
AB-Nic
Number of transitions
F
% time in light side
G
Latency to first entry in light (sec)
H
Control-NaCl +
AB-NaCl + MEC
Control-Nic + MEC
AB-Nic + MEC
###
I
J
#
K
Number of somatic signs
***
###
L
*

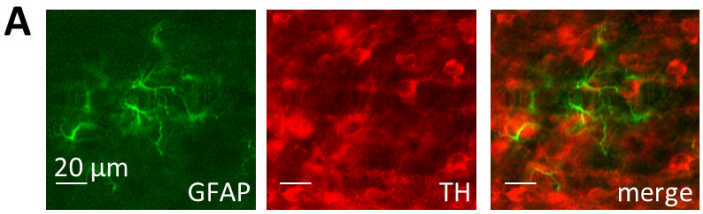
A
20 µm
GFAP
TH
merge

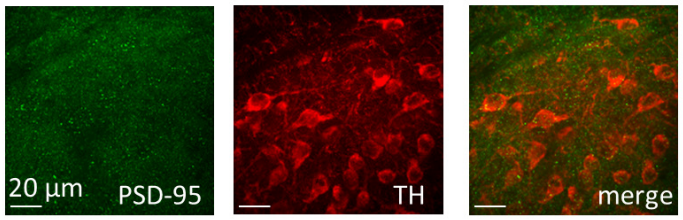
F
20 µm
PSD-95
TH
merge

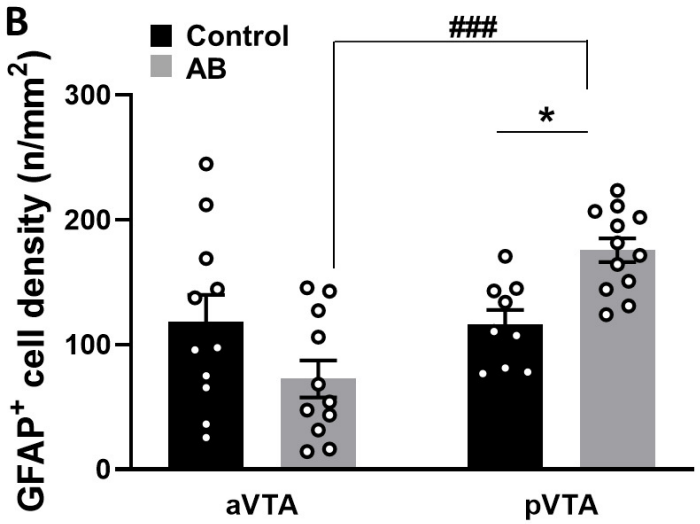
B
Control
AB
###
*
GFAP+ cell density (n/mm2)
300
200
100
0
aVTA
pVTA

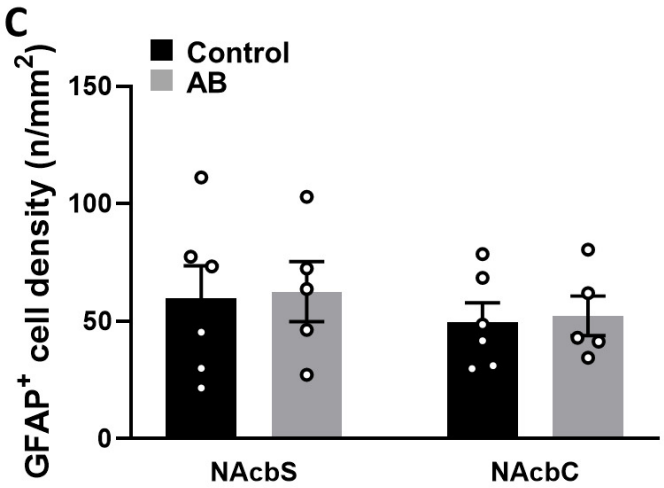
C
Control
AB
GFAP+ cell density (n/mm2)
150
100
50
0
NAcbS
NAcbC

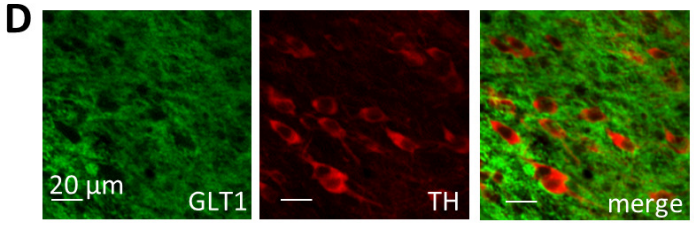
D
20 µm
GLT1
TH
merge

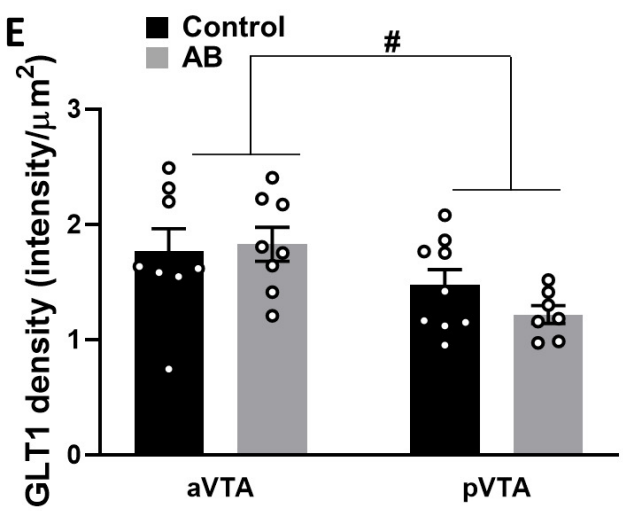
E
Control
AB
#
GLT1 density (intensity/µm2)
3
2
1
0
aVTA
pVTA

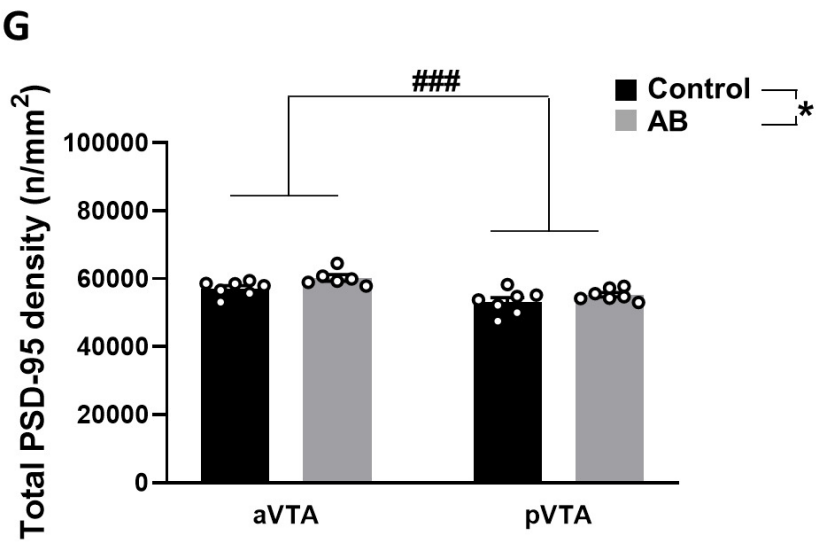
G
###
Control
AB
*
Total PSD-95 density (n/mm2)
100000
80000
60000
40000
20000
0
aVTA
pVTA

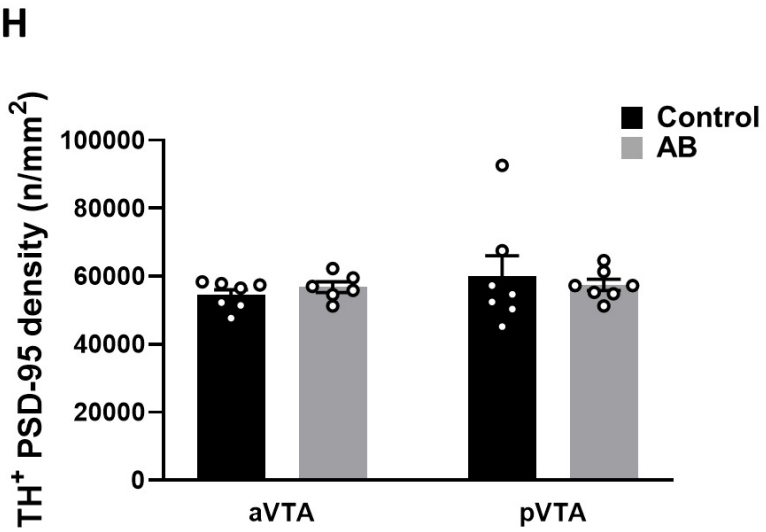
H
Control
AB
TH+ PSD-95 density (n/mm2)
100000
80000
60000
40000
20000
0
aVTA
pVTA

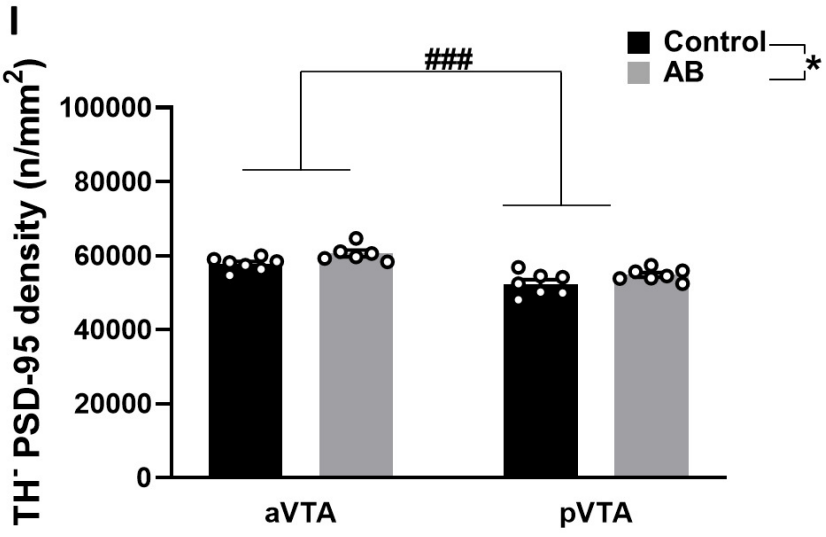
I
###
Control
AB
*
TH- PSD-95 density (n/mm2)
100000
80000
60000
40000
20000
0
aVTA
pVTA

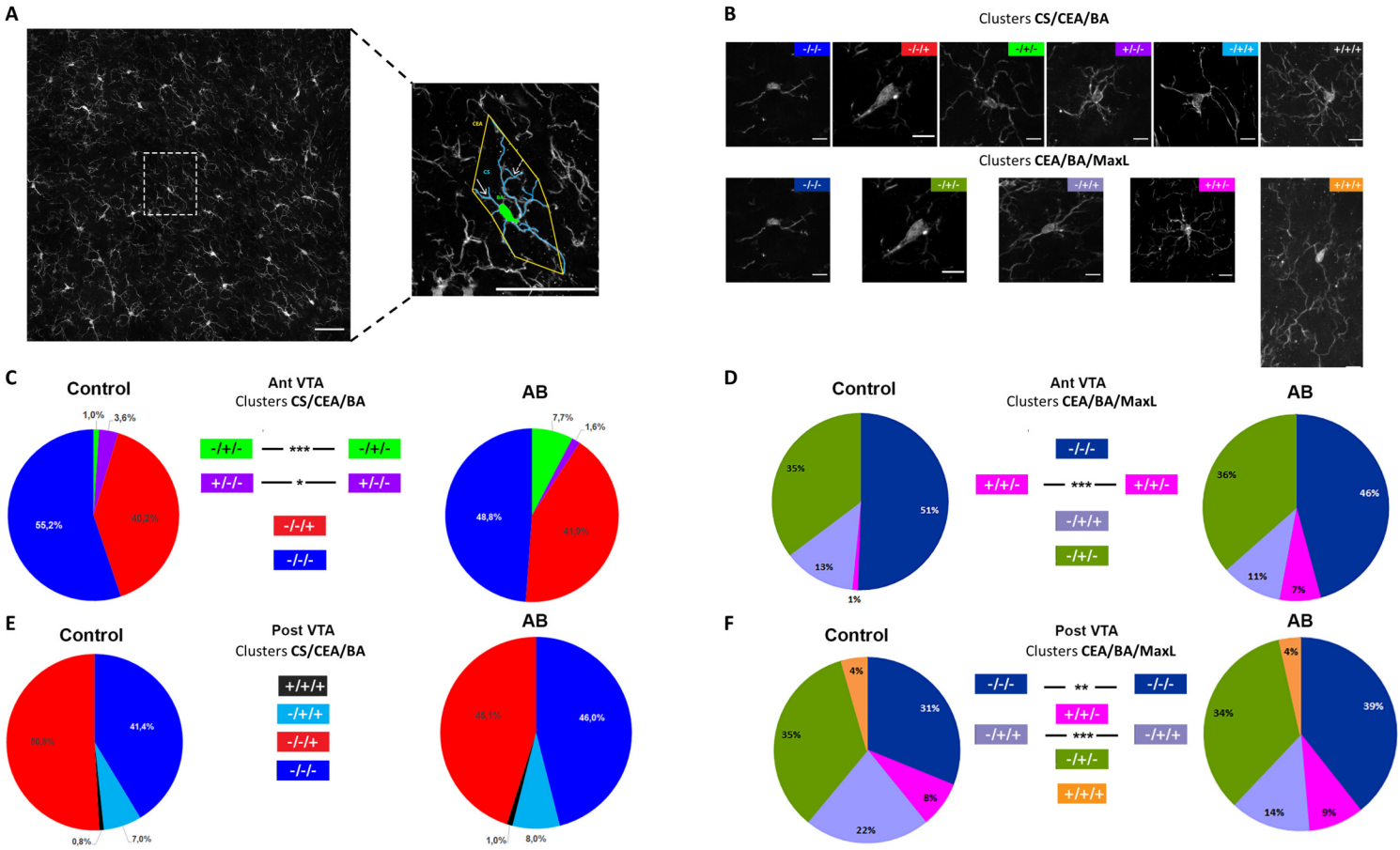
A
B
Clusters CS/CEA/BA
-/-/-
-/-/+
-/+/-
+/-/-
-/+/+
+/+/+
Clusters CEA/BA/MaxL
-/-/-
-/+/-
-/+/+
+/+/-
+/+/+
C
Control
1,0%
3,6%
55,2%
40,2%
Ant VTA
Clusters CS/CEA/BA
-/+/-
***
-/+/-
+/-/-
*
+/-/-
-/-/+
-/-/-
AB
7,7%
1,6%
48,8%
41,9%
D
Control
35%
51%
13%
1%
Ant VTA
Clusters CEA/BA/MaxL
-/-/-
+/+/-
***
+/+/-
-/+/+
-/+/-
AB
36%
46%
11%
7%
E
Control
50,8%
41,4%
0,8%
7,0%
Post VTA
Clusters CS/CEA/BA
+/+/+
-/+/+
-/-/+
-/-/-
AB
46,1%
46,0%
1,0%
8,0%
F
Control
4%
31%
35%
8%
22%
Post VTA
Clusters CEA/BA/MaxL
-/-/-
**
-/-/-
+/+/-
-/+/+
***
-/+/+
-/+/-
+/+/+
AB
4%
39%
34%
14%
9%